© Universiti Tun Hussein Onn Malaysia Publisher's Office

IJIE

http://penerbit.uthm.edu.my/ojs/index.php/ijie
ISSN : 2229-838X e-ISSN : 2600-7916

The International Journal of Integrated Engineering

Performance Analysis of Optimized Screen-Printed Electrodes for Electrochemical Sensing

Nurul Amira Farhana Roslan[1], Rosminazuin Ab Rahim[1*], Aliza Aini Md Ralib[1], Nor Farahidah Za'bah[1], Anis Nurashikin Nordin[1], Mohd Saiful Riza Bashri[1], Muhammad Irsyad Suhaimi[2], Zambri Samsudin[2], Lim Lai Ming[2], Gandi Sugandi[3]

[1]Department of Electrical and Computer Engineering, Kulliyyah of Engineering,
International Islamic University Malaysia, Gombak, Kuala Lumpur, 53100, MALAYSIA

[2]Jabil Circuit Sdn. Bhd,
Bayan Lepas Industrial Park Phase 4, Penang, 11900, MALAYSIA

[3]Research Center for Electronics and Telecommunications,
National Research and Innovation Agency (BRIN), Jl Cisitu, Sangkuriang, Bandung, Jawa Barat, INDONESIA

*Corresponding Author

DOI: https://doi.org/10.30880/ijie.2022.14.03.027
Received 15 January 2022; Accepted 07 June 2022; Available online 20 June 2022

Abstract: The screen-printed electrode (SPE) sensor is widely employed in food analysis, environmental health monitoring, disease detection, toxin detection and other applications. As it is crucial for the SPE sensor to have an outstanding performance, this study examined the effects of manipulating the working electrode (WE) radius, gap spacing between electrodes, and counter electrode (CE) width on the performance of an SPE sensor. Finite element simulation on various geometrical dimensions was done prior to screen-printed electrode SPE sensor's fabrication at Jabil Circuits Sdn Bhd. The electrodes performance is measured through cyclic voltammetry (CV) using a potentiostat at an optimum scan rate of 0.01 V/s and a voltammetry potential window range of -0.2 to 0.8 V in 0.01 M Phosphate Buffered Saline (PBS) solution. It is discovered that adjusting the WE area and the gap separation between the electrodes had the most impact on sensor performance compared to varying the CE width. In both simulation and CV measurements, WE with the highest radius of 0.9 mm with an effective area of 2.54 mm^2, and the smallest gap spacing of 0.7 mm has shown the highest current density of 0.04 A/mm^2 (simulation) and 0.3 $\mu A/mm^2$ (experiment) which can be translated as the highest sensitivity for the SPE sensor. Further CV measurement in nicotine sensing application has proven that the SPE sensor can effectively detect the nicotine oxidation indicating its promising potential as a biosensor. Combination of optimum SPE dimension together with suitable electrode modification process serves as the basis for an effective and sensitive SPE sensor for various biosensing applications.

Keywords: Screen-printed electrode, sensor, area, spacing, simulation, voltammetry, performance, current density

1. Introduction

Sensors with high sensitivity, selectivity, and efficiency are becoming more important in today's world. Most of the conventional sensors and detectors involve bulk and expensive instruments such as chromatography-mass spectrometry (GC-MS), capillary-electrophoresis mass spectrometry (CE-MS), and high-performance liquid chromatography (HP-LC), which may need additional pre-treatment [1]–[3]. Thus, electrochemical-based screen-printed electrode (SPE) sensors fabricated using screen-printing technology have emerged as a promising and cheap alternative to the complex

*Corresponding author: rosmi@iium.edu.my

chromatography and spectrometry technology, due to its ease of use and quick analysis time. The total performance of an electrochemical SPE sensor is determined by the characteristics of the electrodes, and therefore the optimal SPE sensor's characteristics must be chosen to maximize the sensor's efficiency. In other words, the design, material, and type of electrodes have a significant impact on the quality of SPE sensors. This type of sensor will be examined from various perspectives, including the electrode design, material selection, main parameters, and fabrication method [4]–[6].

In recent years, many applications in industries such as medicine and healthcare, clinical research, and agriculture are utilizing screen-printed sensors integrated with electrochemical systems due to their many advantages [7], [8]. One of the well-known SPE sensors is the glucose sensor to diagnose and treat diabetes by measuring the patient's glucose levels [9]. Another example of an SPE sensor in the medical industry is the nicotine sensor which is used to detect nicotine levels of smokers and ex-smokers [10].

Aside from the low cost and the mass production, the most important feature of SPE sensors is the size of the microelectronic, which allows the amount of sample used for analysis to be reduced to as little as a few microliters. This SPE's key feature enables the monitoring instrument to be connected to the portable instruments while minimizing the total size of the electrochemical sensor device [6], [7]. For biosensing applications, the electrodes particularly WE play a significant role in which the bioanalytical interaction and its electrochemical process take place. As such, in improving the SPE sensors' overall performance, concentrated research efforts are found to be dealing with electrodes modification such as adding metal compounds [11], pre-treating electrodes [12], performing mechanical activation [13], and adjusting the design parameters [14].

The SPE has been used in many applications due to its design and material flexibility. To improve the performance of these SPE sensors, the ideal structures, and geometrical dimensions must be explored [15]. However, many recent studies concentrate on electrode modifications to improve the SPE sensor's performance. Metal oxides, polymers, carbon nanotubes, and graphene are among the active materials that have been employed to modify the electrodes. There is still a lack of research on optimizing the SPE design parameters and how it influences the electrochemical sensing capability. Few studies on optimizing SPE design parameters are found but most of them are restricted to simulation and modeling only, without considering its performance experimentally [8], [16], [17].

In this research, we investigated the effects of varying the SPE dimensions through simulation works as well as experimental measurements. This investigation is crucial because the fabrication of various electrode geometrical dimensions which cannot be achieved using commercial SPE will experimentally verify the effect of having optimum SPE design on the sensor's performance, thus paving the way forward for its development for biosensing applications.

2. Methodology

Since an optimum SPE design will ensure high electro-migration of ions mobility in the electrochemical process, this study considers various combinations of SPE geometrical dimensions such as the width of the CE, the gap between the CE and WE, and the radius of the WE. This study involves the investigation of these design parameters through COMSOL simulation as well as electroanalytical measurements of various design measurements of Carbon-Silver-SPEs in the presence of salt. In COMSOL simulation, the sensor's performance is measured in terms of the current density while in electroanalytical measurement, the reduction and oxidation processes that occurred on these SPEs are represented by cyclic voltammetry (CV) measurement. The overall flow of the outlined methodology is illustrated in Fig. 1.

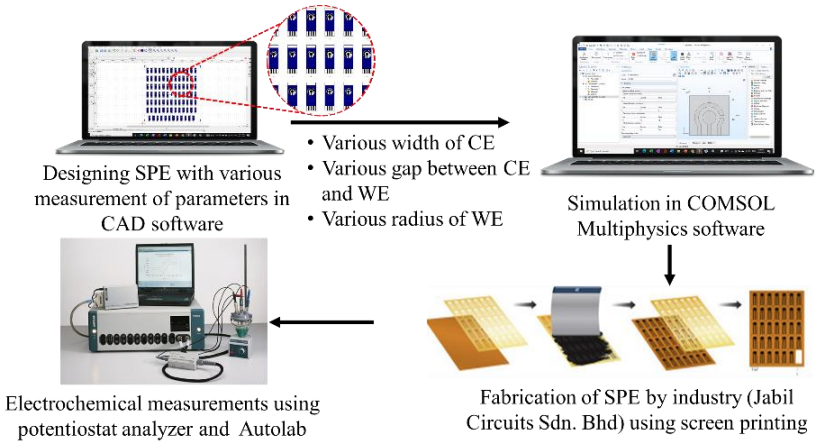

Fig. 1-The overall flow of the outlined methodology

2.1 Chemicals and Apparatus

The phosphate buffer saline (PBS) tablets, Potassium Hexacyanoferrate (II) Trihydrate powder, KCl powder, and standard solution of nicotine were purchased from Sigma-Aldrich. Deionized water was used for all solution preparation. PBS and PBS with nicotine solutions were used as supporting electrolytes and were prepared just before measurement and stored in the dark to prevent oxidation.

In this work, the SPE sensors with various geometrical dimensions were fabricated by Jabil Circuits Sdn. Bhd. which consists of three electrodes: WE, CE, and reference electrode (RE). The WE are dominant over the other electrodes because it is the active area where immobilized agents aim to identify the electrochemical events such as oxidation and reduction (redox). Meanwhile, the RE and CE are needed to maintain the potential of the WE and complete the circuit [6], [18]. For each electrode, carbon and silver were utilized as materials in this study. Carbon was chosen as CE and WE because it is an affordable chemical inert material that can be modified to increase its performance [19]. Silver was applied as RE because of its high conductivity and low resistance, making it an excellent conductor [19]–[21].

2.2 Design and Fabrication of SPE at Various Geometrical Dimensions

Depending on the application, the shape, pattern, and material of the SPE can all be changed to suit our preferences and demands. In this work, the three-electrodes are printed on top of a thin plastic substrate as a planar system as illustrated in Fig. 2. As illustrated in both the cross-section and top view of the electrochemical sensor design, the electrochemical reactions are triggered when antigens/antibodies from the analyte are deposited at the working electrode during electrochemical measurements of a sensor, interrupting the current in the electrode and electrolyte system. This behavior demonstrates how different surface areas of the electrode and electrolyte system affect current density. [22]–[24].

The SPE sensors reported in this paper were designed in 2D drawings using QCAD software, incorporating references to several commercial sensor designs and existing SPE sensor studies [6], [7], [18], [25]. There were 28 sets of SPE design at various gaps between the electrodes, various radii of the WE, and various widths of the CE. The size range of each parameter used in this research is tabulated in Table 1. The sensor size was designed in 10 mm of width and 30 mm of length and was standardized for all 28 sets of sensors. It is worth noting that the gap between the three-electrode extended legs and its width is fixed to 1 mm to make it easier for the SPE sensor to be connected to a portable device and used with commercial connectors.

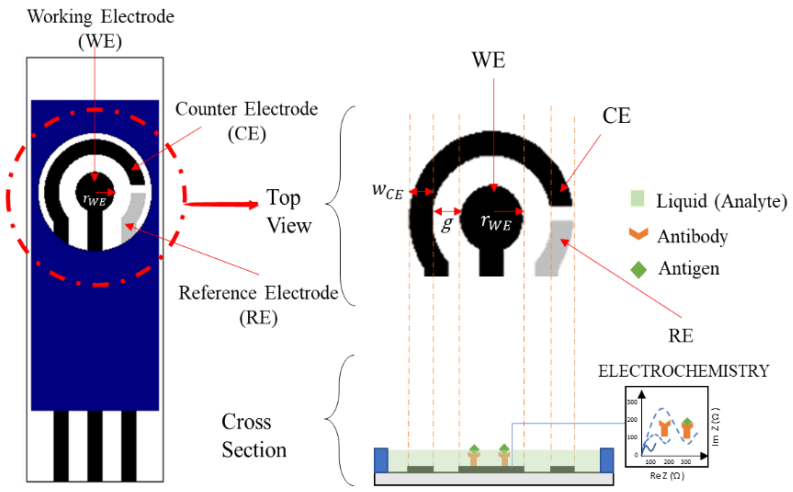

Fig. 2 - Cross-section and top view of the electrochemical sensor with biosensing application [16]

Table 1 – Range of SPE geometrical dimensions

Design Parameters	*Gap, g*	*The radius of WE, r_{WE}*	*Width of CE, w_{CE}*
Range Value	0.7 mm, 1 mm, 1.3 mm	0.9 mm, 1.1 mm, 1.4 mm, 1.7 mm, 2 mm	0.7 mm, 1 mm, 1.3 mm

2.3 COMSOL Simulation and Butler-Volmer Theory

The results of varying the geometrical dimensions were obtained using the finite element method in COMSOL Multiphysics software in terms of current density. The model was chosen from COMSOL's electrical AC/DC 3D simulation module. Because it is ideal for computing electric fields and modeling potential distributions in a conducting medium with negligible inductive effects, the electric current (ec) was chosen as the physics in this simulation. COMSOL evaluates the equation of conduction and displacement current continuity, as well as the free induction effects, as indicated in Equation 1 [26]

$$-\nabla.\left((\sigma + j\omega\,\varepsilon_r\,\varepsilon_0\,)\,\nabla V\,\right) = 0 \tag{1}$$

where, σ is the conductivity, ω is the angular frequency, ε_0 is the vacuum permittivity, ε_r is the material relative permittivity, and V is the potential. The electric field, E and displacement, D can be obtained from the gradient of V from Equation 2 and 3:

$$E = -\nabla V \tag{2}$$

$$D = \varepsilon_r\,\varepsilon_0\,E \tag{3}$$

As shown in Fig. 3 (a), only WE and CE are simulated in this simulation at various geometrical dimensions. The RE is excluded because its primary function is to complete the circuit and maintain the constant voltage generated by both the CE and the WE [7]. The input elements required in the COMSOL simulation are listed in Table 2. A global parameter of the gap size was set at 0.7 mm to avoid measurement interference from other electrodes during the gap size adjustment. The parametric sweep range is defined to be between 0.7 and 1.3 mm. Aside from the gap dimensions, the same analyses were performed using a specified working area with a radius of 0.9 mm to 2 mm. The physics-controlled mesh sequence type was used for this simulation to produce more accurate results, and the mesh element size was set to extremely fine, as shown in Fig. 3 (b).

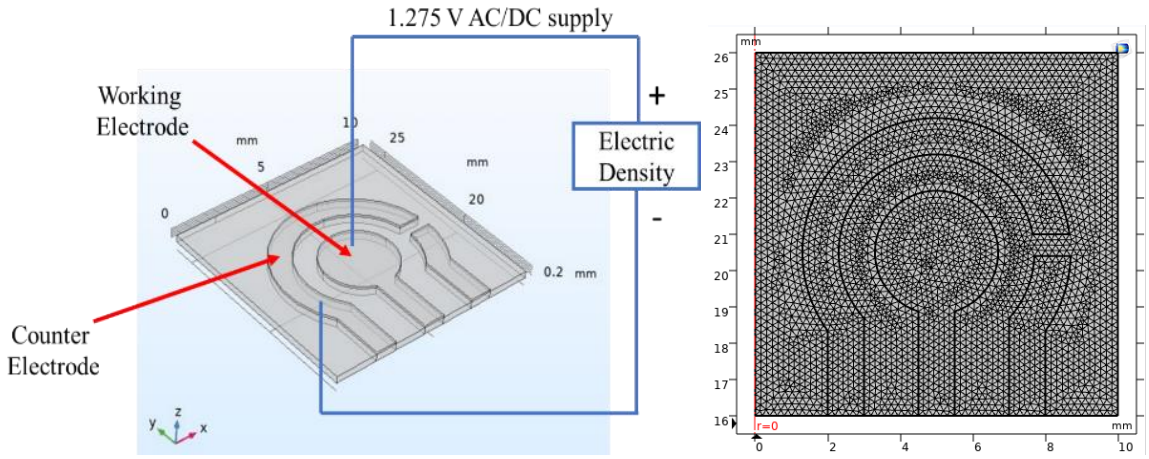

Fig. 3 – (a) Working area defined in COMSOL; (b) Extremely fine-meshed working area

Table 2 - Parameters used in COMSOL simulation

Parameter	*COMSOL SIMULATION*		
	Definition	***Value***	***Unit***
r_{WE}	The radius of Working Electrode	0.9, 1.1, 1.4, 1.7, 2	mm
g	Gap Spacing Between WE and CE	0.7, 1.0, 1.3	mm
w_{CE}	Width of Counter Electrode	0.7, 1.0, 1.3	mm
V1	Voltage Applied	1.275	V
cond_water	Electrical Conductivity of Water	$5.5e^{-6}$	S/m
perm_water	Relative Permittivity of Water	80	1
cond_carbon	Electrical Conductivity of Carbon	$3e^{5}$	S/m
perm_carbon	Relative Permittivity of Carbon	12	1

Butler-Volmer's theory as represented in Equation 4 used to analyze the relationship between current density and total capacitance over the electrode surface area [8]. According to this theory, capacitance is proportional to current density, which means that as total capacitance increases, current density begins to increase as well. Furthermore, because the active geometric area is inversely proportional to current density, reducing the size of the WE geometric area increases current density while also improving the SPE sensor's sensitivity.

$$i_0 = \frac{I_{sensor}.CPE.j\omega.V_{applied}}{A_{geo.}\{e\left[\frac{(1-\alpha).n.F}{R.T}.(E-E_{eq})\right]-e\left[-\frac{a.n.F}{R.T}.(E-E_{eq})\right]\}} \quad (4)$$

i_0 = current density, A/m^2
A_{geo} = area of electrode active geometry, m^2
I_{sensor} = total sensing current, A
C_{total} = CPE = total capacitance, F
E = electrode potential, V
$V_{applied}$ = applied potential, V
E_{eq} = equilibrium potential, V
T = absolute temperature, K
n = number of electrons involved in reaction
F = Faraday constant = 96485 C mol^{-1}
R = universal gas constant = 8.3145 J/mol.K
α = symmetry factor

2.4 Samples Preparation

The 0.01 Phosphate buffered saline (PBS) solution used in this work was prepared by dissolving a PBS tablet into 200 ml of deionized water. For PBS with nicotine, 0.1 ml of standard nicotine solution was drop-casted into 20 ml of PBS solution. Both prepared solutions were stored at 4 °C in laboratory freezer for later use in experiments.

The Ferricyanide solution was prepared in an Eppendorf tube by dissolving the 0.15 g of KCl powder and 0.04 g of potassium hexacyanoferrate (II) trihydrate powder into 20 mL of deionized water. Then, the tube was capped and mixed the solution by swirling the tube until translucent pale yellow appeared, and the solution was stored in the darkroom.

2.5 Measurement of Cyclic Voltammetry

All electrochemical SPE sensors fabricated were tested using a three-electrode setup on an Autolab PGSTAT128N potentiostat (Metrohm AG, Switzerland). As shown in Fig. 4, the SPE sensor was attached to standard cell cables to the potentiostat device which is later connected to NOVA 2.1 software. To keep the pH stable and to provide ions for the electrochemical studies, a buffered solution is employed in this work. The SPE sensor's WE are then completely immersed in the beaker containing 15 ml of PBS solution, 15 ml of PBS with nicotine, and 15 ml of Ferricyanide solution. The buffered solution, which contains salt ions, migrates to balance the charge, and completes the electrical circuit during the electrons transferred at WE of the electrodes.

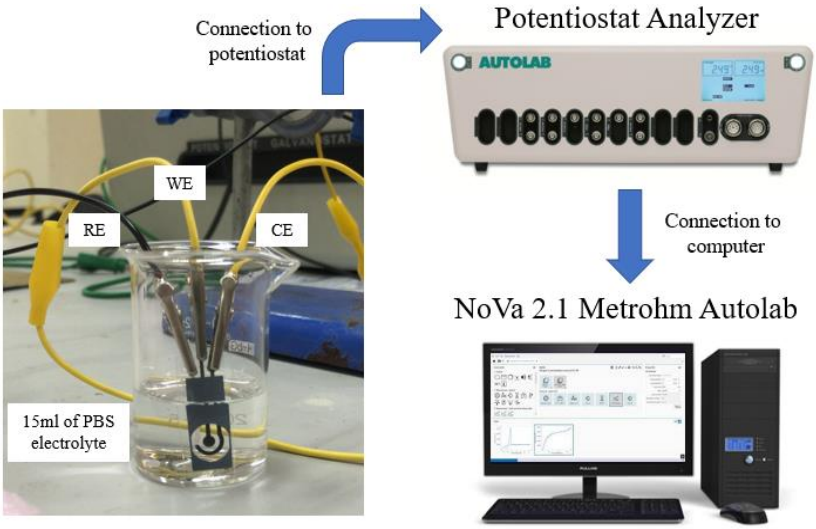

Fig. 4 - Experiment setup for electrochemical CV measurement

3. Results and Discussion

The three-electrode SPE sensors and their electrochemical evaluation were explored through simulation in COMSOL software as well as through experimental studies of CV measurement in 0.01 M PBS solution. In CV measurement, the current generated when the potential is changed from 0.3 V to -0.2 V, then to 0.8 V, then back to the initial potential, shows the electrochemical properties of the analyte. The maximum or peak current must be as high as possible during CV scanning. Since peak currents are the key parameters for a CV, the final comparison of the CV peak currents of the fabricated SPE sensors with various geometrical dimensions was performed to compare the sensor's performance in terms of current density [18].

The simulation and CV measurement works are employed to compare the effect of various combinations of electrodes' geometrical dimensions on the current density and the electrochemical performance of the sensors. Thus, the sensors are grouped according to their gap spacing between the electrodes, the radius of the WE, and the width of the CE.

3.1 Simulation works

COMSOL simulation is performed to investigate the effects of varying electrodes' geometrical dimensions on the SPE sensor's performance using an AC/DC 3D simulation module. Another investigation is done on the SPE sensor's electrochemical behavior 1D Electrochemical simulation module.

3.1.1 Current Density Simulation using AC/DC 3D module

Fig. 5 shows the current density measurement point at the edge of WE and CE, which is represented with a red line between points a and b. According to the simulation results presented in Fig. 6 (a), the smallest gap of 0.7 mm between the two electrodes enhanced the current density due to the interference of the electric field of the asymmetrical design, while the largest gap of 1.3 mm contributed to the lowest value of current density. Additionally, as shown in Fig. 6 (b), the current density of the SPE sensor is decreases when the size of the WE radius is increased, starting from 0.9 mm to 2.0 mm. It is because increasing the electrode's area (particularly WE radius) will significantly reduce the current value over a specific area. However, altering the width of the CE from 0.7 mm to 1.3 mm does not affect the magnitude of current density, implying that the CE width does not affect the performance of the SPE sensor. As demonstrated in Fig. 7, regardless of the width of CE, the current density remains constant. Because the space between the extended legs of the constructed SPE sensor was set at 1 mm, the width of 1 mm was chosen as the best dimension. In summary, SPE sensors with a smaller WE radius and smaller electrodes gap will produce higher current density, which indicates better sensors' performance.

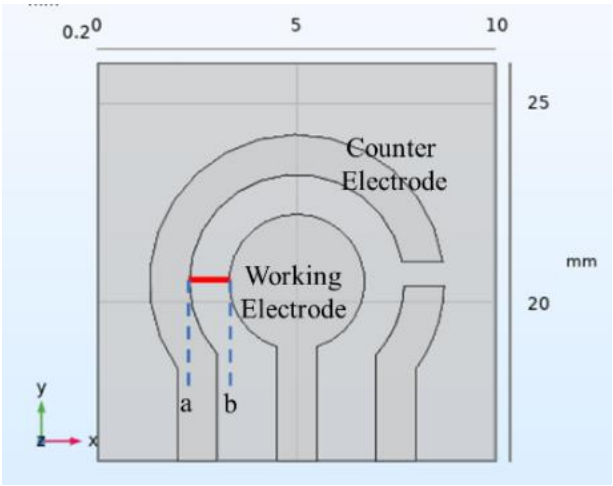

Fig. 5 - A red line between a and b indicates the location of the measured current density

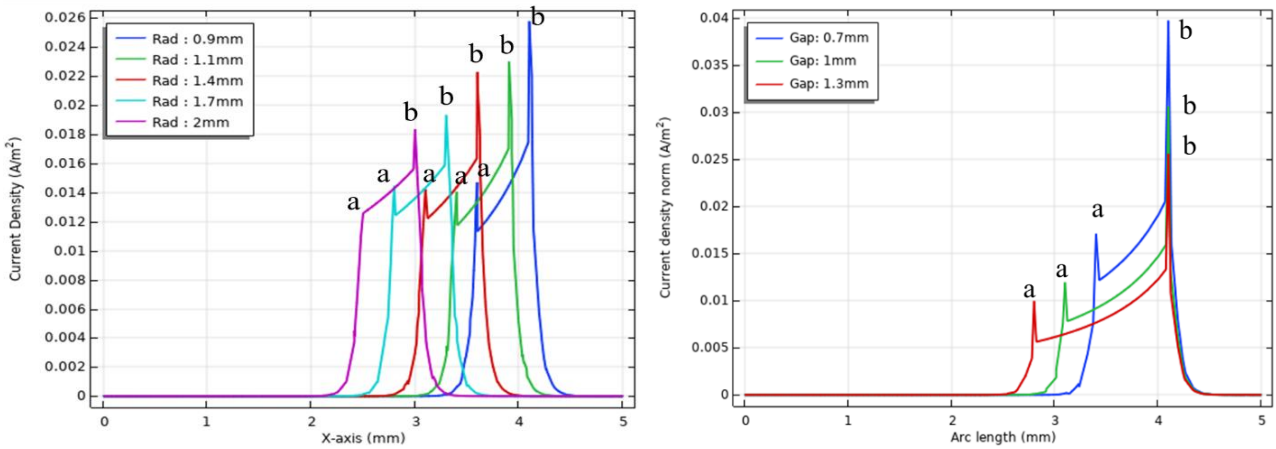

(a) (b)

Fig. 6 – (a) Current density at various WE radius (Gap 0.7 mm, Width 1.0 mm); (b) Current density at various electrodes gap (WE radius 0.9 mm, Width 1.0 mm)

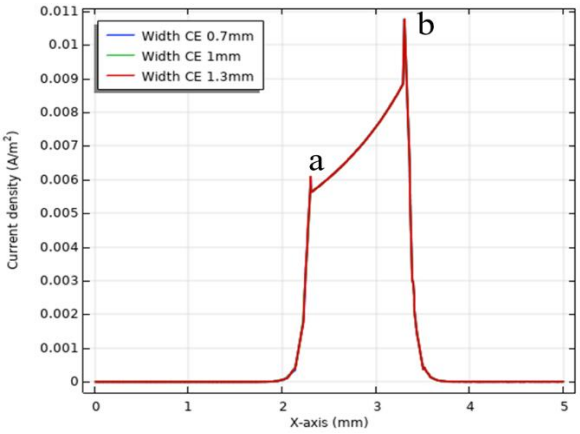

Fig. 7 - Current density at various CE widths (Gap 0.7 mm, WE radius 0.9 mm)

3.1.2 Electrochemical Process using 1D Electrochemical Module

In this work, WE of 0.9 mm radius was simulated for the electrochemical process as it has been chosen as the optimal dimension in prior simulation works. The CV of the SPE sensor is shown in Fig. 8 at different scan rates ranging from 0.001 V/s to 0.5 V/s. The variation of peak currents versus potential scan rates was examined using these CVs. From the simulation results, it is shown that the anodic and cathodic peaks are increasing with increasing scan rates, as seen in Fig. 8(a). The redox peak current density varied with the square root of the scan rate, is shown in Fig. 8(b). It is observed that the plots of redox peak current density are linearly dependent on the square root of scan rate ($v^{1/2}$) at all scan rates with high correlation coefficients (R^2) of 0.9995 and 0.9996. The fact that the correlation coefficient is high ($R^2 \approx 1$) and linearly dependent on $v^{1/2}$ in this simulation indicates that the redox process is diffusion-controlled. According to the theory, the variation of current peaks is linear with the scan rate, v in the case of adsorbed molecules. As a result, in the case of molecules in solution, the current peaks vary linearly with the square root of the scan rate, $v^{1/2}$ [8], [27].

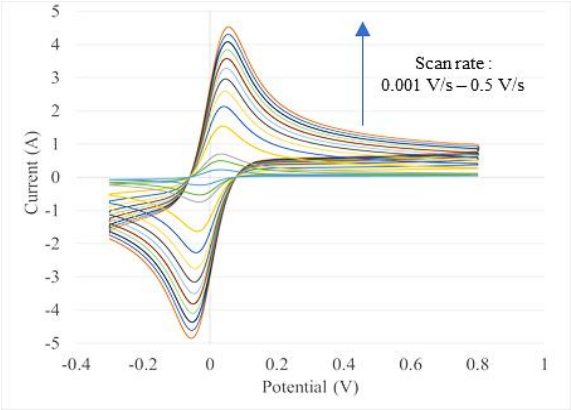

(a)

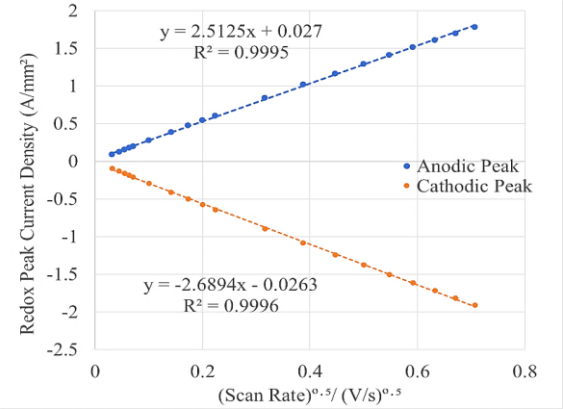

(b)

Fig. 8 – (a) The current density magnitude of gap: 0.5 mm; (b) the current density magnitude of radius WE: 0.9 mm

3.2 Experimental measurements

CV measurements on the prepared samples are performed in 0.01 M PBS solution using Autolab potentiostat. The measurement results on different electrodes gap, WE radius as well as CE width are reported in this section. The CV measurements are also performed for different materials (carbon and silver) of CE tracking lines. Further measurement is done for nicotine detection applications to observe the sensing capability of the fabricated SPE sensors.

3.2.1 The Effects of Electrodes Gap on Cyclic Voltammetry

Fig. 9 shows the CV of 0.01 M PBS for various gap sizes at three different values of 0.7, 1.0, and 1.3 mm. The anodic and cathodic peaks in Fig. 9 (a) become higher as the gap between the WE and CE gets smaller. The difference between the large current (oxidation current) and the small current (reduction current) when implementing an SPE sensor with a 0.7 mm gap spacing is 5.142 µA; at 1 mm gap, the difference is 4.162 µA; and at 1.3 mm gap, the difference is 3.981 µA. To obtain the values of current density, the peak currents are divided by the geometric area of the WE (Radius of WE: 2 mm, Area of WE: 12.57 mm²). The relationship between current density and electrode gap is plotted in Fig. 9(b). It shows that when the electrodes gap decreases, the current density increases. It is because the intensity of an electric field is proportional to the separation distance between two charged plates, which in this study is the gap between the WE and CE [15]. This observation agrees with our findings in COMSOL simulation.

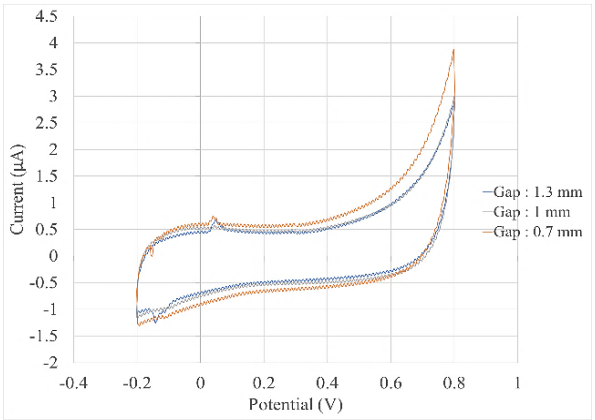

(a)

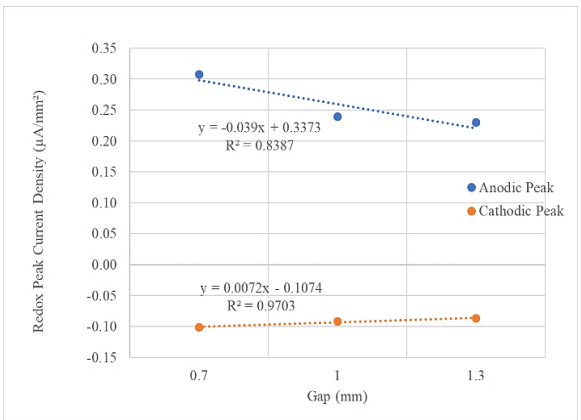

(b)

Fig. 9 – (a) Cyclic voltammetry at various electrodes gaps electrode gaps; (b) Anodic and cathodic peak current at various electrodes gaps

3.2.2 The Effects of Working Electrode's Radius on Cyclic Voltammetry

It was observed that the size of the WE also affects the current after scanning with CV. The peak current increases as the WE radius increases in size, as shown in Fig. 10 (a). It is because as the area of the WE increase, higher amounts of salt ions from the PBS solution are polymerized on the surface, leading to higher amounts of salt being integrated. As the quantity of hybridization events is related to the electroreduction current generated during the detection phase, it was determined that the current could be adjusted by controlling the amount of salt ion integration at the WE [15]. The relationship between current density and WE radius is shown in Fig. 10 (b). Since the current density increases as the radius decreases, the SPE sensor will be more sensitive when the size of WE are smaller. The difference between the maximum and minimum currents is tabulated in Table 3. These findings are also in good agreement with the results obtained from the COMSOL simulation.

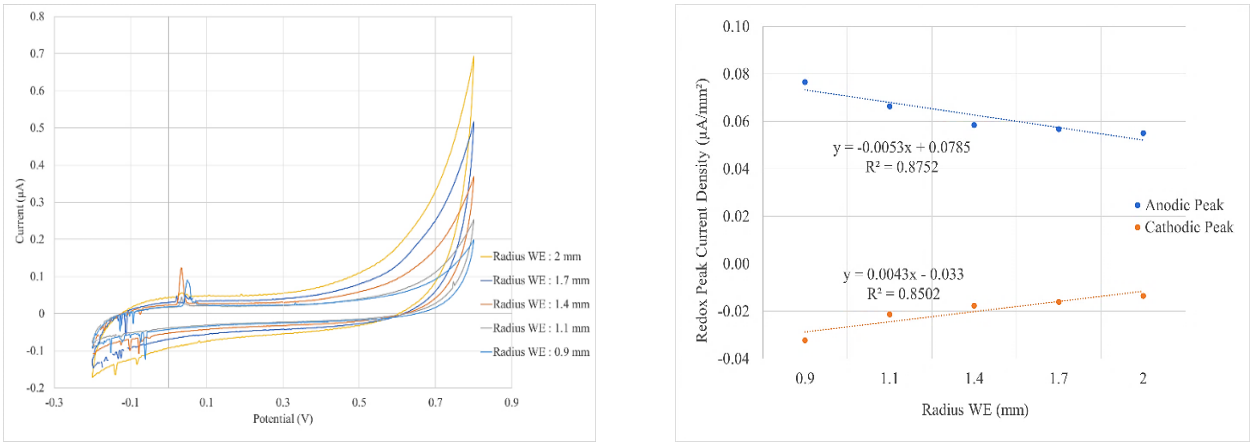

(a) (b)

Fig. 10 – (a) Cyclic voltammetry at various WE radius; (b) Anodic and cathodic peak currents at various WE radius

Table 3 - Peak difference between the maximum and minimum currents with the corresponding radius

Radius of WE (mm)	*Area of WE (mm²)*	*Peak Difference (μA)*
0.9	2.54	0.277
1.1	3.80	0.334
1.4	6.16	0.469
1.7	9.08	0.661
2.0	12.57	0.862

3.2.3 The Effects of Counter Electrode's Width on Cyclic Voltammetry

It is worth noting from the simulation results of current density at various CE widths conducted in Section 3.1, no change in current density was observed at various CE widths. However, in the CV measurement, as the width of the CE changes, the voltammogram in Fig. 11 indicates different peak oxidation and reduction currents. The peak currents increase in response to the increased width of the CE, as shown in Fig. 11 (a). When testing an SPE sensor with a 0.7 mm counter width, the difference of anodic and cathodic currents is 4.162 μA; for width 1 mm, the difference is 7.051 μA; and for width 1.3 mm, the difference is 16.425 μA. Its indicates that a higher current is observed at higher CE width. This also means that in the electrochemical reaction, the CE has completed the circuit by collecting the electroreduction current generated at the WE, resulting in a constant voltage at the WE relative to the RE [15]. The relationship between current density and CE width is depicted in Fig. 11 (b). The plotted result shows that as the width of the CE is increased, the current density increases, meaning that the SPE sensor has more sensitivity. The difference in the value of current density in both simulation and measurement is likely due to the different properties of the material used in COMSOL's library and material used during the fabrication process done at Jabil Circuit Sdn. Bhd.

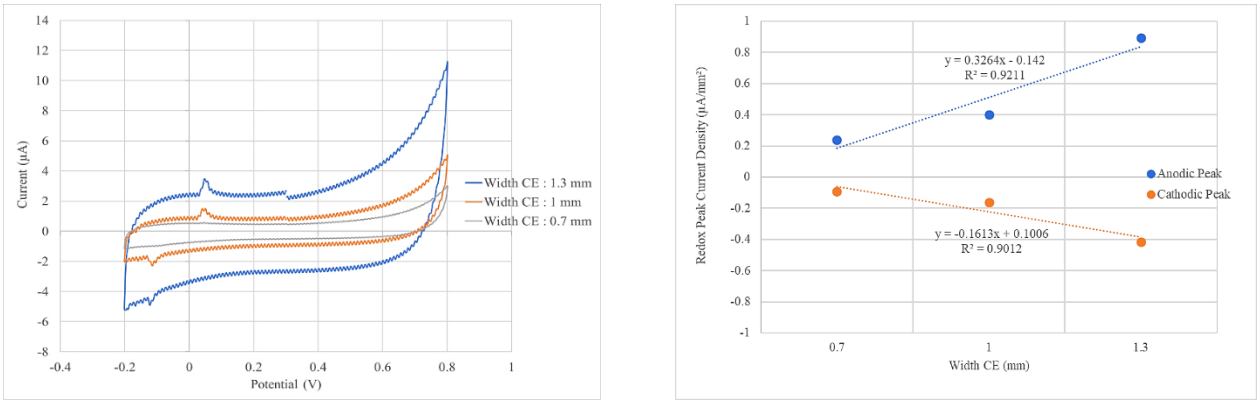

(a) (b)

Fig. 11 - (a) Cyclic voltammetry at various CE width; (b) Anodic and cathodic peak current at various CE width

3.2.4 The Effects of Silver vs Carbon Tracking Lines on Cyclic Voltammetry

To investigate the effects of using different materials on the CE tracking line, the three-electrode SPE sensors are fabricated with both carbon and silver tracking lines as shown in Fig. 12 (a). Fig. 12 (b) shows the corresponding CV for both CE tracking lines at various WE radius. In general, it can be observed that the peak of currents (at various WE radius) of the carbon tracking line have relatively larger values than the peak of currents of the silver tracking line (at various WE radius). It could be due to the properties of carbon materials, which are stable and provide great electrochemical performance with high preservability when the CV is applied. It can be concluded that the carbon CE tracking line offers higher sensitivity of SPE sensors than the silver CE tracking line.

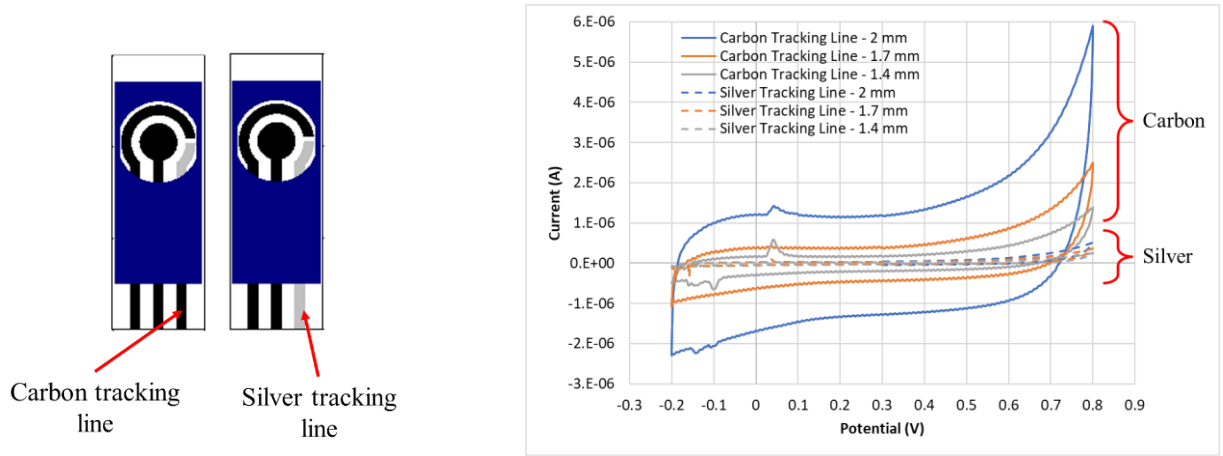

(a) (b)

Fig. 12 – (a) SPE sensor with carbon tracking line and silver tracking line; (b) CV of carbon and silver tracking line

3.3 Cyclic Voltammetry of Nicotine Detection on SPE sensors

The electrochemical behavior of nicotine oxidation on the SPE was investigated using CV measurement. Fig. 13 shows the respective voltammograms of the fabricated SPE sensors in the absence and presence of nicotine in PBS. During the anodic scan, nicotine undergoes oxidation at the surface of the SPE starting at a potential of 0.3 V and exhibiting a high oxidation peak current at 0.8 V compared to the blank PBS when no nicotine was added. During the cathodic scan, no voltammetric response in correspondence to the nicotine reduction was found when the voltage was reversed at -0.2 V. As a result, it can be concluded that nicotine oxidation at the SPE is irreversible, as revealed by previously published results [10], [25]. It can also be summarized that nicotine detection can be performed using the fabricated SPE sensors which proves its sensing capabilities.

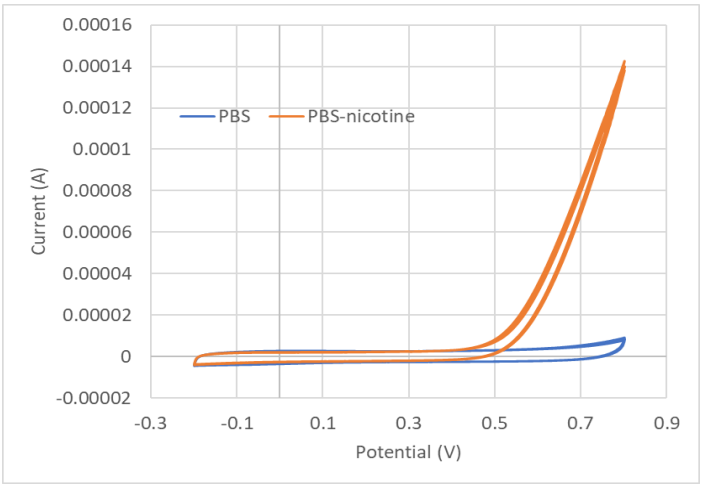

Fig. 13 - Cyclic voltammograms of the fabricated SPE in the absence and presence of 1 M nicotine in 0.1 M PBS at a scan rate of 0.1 V/s

4. Conclusions

The screen-printing technology offers a variety of options to fabricate the three-electrode SPE sensors. Variations in design parameters such as gap separation between electrodes, radius of WE, and width of CE are simple to implement. The three-electrode SPE sensor system was successfully designed, simulated, and fabricated, in this study. Later, the final evaluation by COMSOL simulation, capacitance measurement, and electrochemical measurement with cyclic voltammetry analysis was conducted.

During simulation, it was discovered that varying the gap between electrodes as well as the radius of the WE influence the current density value. The maximum peak current density of 0.04 A/mm^2 was achieved by combining the smallest electrodes gap of 0.7 mm with the smallest WE radius of 0.9 mm. It also shows that varying the width of the CE does not affect the SPE sensor's performance, since the value of current density remains unchanged regardless of the counter width.

For electrochemical sensing, the optimal radius of WE was 0.9 mm, and the optimal gap was found to be 0.7 mm since it produced the highest current density of 0.3 μA/mm^2 to enhance electro-migration of ions at the three-electrode SPE sensor interfaces. Besides, for the width of the CE, the electrochemical sensing shows that the largest counter width of 1.3 mm has the highest current density value. The width of 1 mm was chosen as the ideal and acceptable dimension to standardize the width with the extended electrodes. It is sufficient to complete the circuit because the primary function of the CE is to maintain the potential of the WE at a constant potential relative to the RE.

In conclusion, by optimizing the electrodes' geometrical dimensions, the performance of the three-electrode SPE sensor based on electrochemical detection can be improved. This method of improving the performance of SPE sensors has the advantages of being simple, less expensive, and requiring low sample amounts. The CV measurements results of nicotine detection have proven the fabricated SPE sensing capabilities. The actual benefit of optimized geometrical parameters of a three-electrode SPE sensor to achieve optimum performance is its lower cost as compared to other electrode modifications such as changing the electrode material and performing some pre-treatment on the SPE sensor, which requires additional chemicals and equipment. However, by combining these optimal SPE geometrical dimensions with additional electrodes modification processes such as using active materials and electrode pre-treatment on the SPE surface, the sensor's performance can be improved.

Acknowledgment

This project is sponsored by International Islamic University Malaysia under grant project RMCG20-014-0014. The authors would like to thank Jabil Circuit Sdn. Bhd. for funding the research materials.

References

[1] A. Karthika, P. Karuppasamy, S. Selvarajan, A. Suganthi, and M. Rajarajan, "Electrochemical sensing of nicotine using CuWO4 decorated reduced graphene oxide immobilized glassy carbon electrode," *Ultrason. Sonochem.*, vol. 55, no. December 2018, pp. 196–206, 2019.

[2] A. M. Hossain and S. M. Salehuddin, "Analytical determination of nicotine in tobacco leaves by gas chromatography-mass spectrometry," *Arab. J. Chem.*, vol. 6, no. 3, pp. 275–278, 2013.

[3] V. V. Gholap, L. Kosmider, and M. S. Halquist, "A Standardized Approach to Quantitative Analysis of Nicotine in e-Liquids Based on Peak Purity Criteria Using High-Performance Liquid Chromatography," *J. Anal. Methods Chem.*, vol. 2018, 2018.

[4] H. A. Abdulbari and E. A. M. Basheer, "Electrochemical Biosensors: Electrode Development, Materials, Design, and Fabrication," *ChemBioEng Rev.*, vol. 4, no. 2, pp. 92–105, 2017.

[5] A. A. Bojang and H. S. Wu, "Characterization of electrode performance in enzymatic biofuel cells using cyclic voltammetry and electrochemical impedance spectroscopy," *Catalysts*, vol. 10, no. 7, 2020.

[6] A. Hayat and J. L. Marty, "Disposable screen printed electrochemical sensors: Tools for environmental monitoring," *Sensors (Switzerland)*, vol. 14, no. 6, pp. 10432–10453, 2014.

[7] Z. Taleat, A. Khoshroo, and M. Mazloum-Ardakani, "Screen-printed electrodes for biosensing: A review (2008-2013)," *Microchim. Acta*, vol. 181, no. 9–10, pp. 865–891, 2014.

[8] A. A. Zainuddin, A. N. Nordin, R. A. Rahim, and W. C. Mak, "Modeling of a novel biosensor with integrated mass and electrochemical sensing capabilities," *IECBES 2016 - IEEE-EMBS Conf. Biomed. Eng. Sci.*, pp. 420–425, 2016.

[9] N. S. Ridhuan, K. Abdul Razak, and Z. Lockman, "Fabrication and Characterization of Glucose Biosensors by Using Hydrothermally Grown ZnO Nanorods," *Sci. Rep.*, vol. 8, no. 1, pp. 1–12, 2018.

[10] E. Mehmeti, T. Kilic, C. Laur, and S. Carrara, "Electrochemical determination of nicotine in smokers' sweat," *Microchem. J.*, vol. 158, no. June, 2020.

[11] J. Wang, Z. Xu, M. Zhang, J. Liu, H. Zou, and L. Wang, "Improvement of electrochemical performance of screen-printed carbon electrodes by UV/ozone modification," *Talanta*, vol. 192, no. 2, pp. 40–45, 2019.

[12] M. I. González-Sánchez, B. Gómez-Monedero, J. Agrisuelas, J. Iniesta, and E. Valero, "Highly activated screen-printed carbon electrodes by electrochemical treatment with hydrogen peroxide," *Electrochem. commun.*, vol. 91, no. April, pp. 36–40, 2018.

[13] L. R. Cumba *et al.*, "Can the mechanical activation (polishing) of screen-printed electrodes enhance their electroanalytical response?," *Analyst*, vol. 141, no. 9, pp. 2791–2799, 2016.

[14] J. Prasek *et al.*, "Optimization of planar three-electrode systems for redox system detection," *Int. J. Electrochem. Sci.*, vol. 7, no. 3, pp. 1785–1801, 2012.

[15] D. E. Garcia, T. H. Chen, F. Wei, and C. M. Ho, "A Parametric Design Study of an Electrochemical Sensor," *J. Lab. Autom.*, vol. 15, no. 3, pp. 179–188, 2010.

[16] N. A. Farhana Roslan *et al.*, "Simulation of Geometrical Parameters of Screen Printed Electrode (SPE) for Electrochemical-Based Sensor," *Proc. - 2021 IEEE Reg. Symp. Micro Nanoelectron. RSM 2021*, pp. 137–140, 2021.

[17] H. Kwon and E. Akyiano, "Simulation of cyclic voltammetry of ferrocyanide/ferricyanide redox reaction in the EQCM Sensor," *Comsol.De*, pp. 2–6, 2011.

[18] U. Kavčič and T. Pleša, "the Influence of Printing Properties of Screen Printed Electrodes on Sensitivity Measured With Cyclic Voltammetry," pp. 253–259, 2018.

[19] F. F. Franco, L. Manjakkal, and R. Dahiya, "Screen-Printed Flexible Carbon versus Silver Electrodes for Electrochemical Sensors," *FLEPS 2020 - IEEE Int. Conf. Flex. Printable Sensors Syst.*, pp. 8–11, 2020.

[20] M. Pohanka, "Screen Printed Electrodes in Biosensors and Bioassays. A Review," *Int. J. Electrochem. Sci.*, vol. 15, no. 11, pp. 11024–11035, 2020.

[21] K. Yamanaka, M. C. Vestergaard, and E. Tamiya, "Printable electrochemical biosensors: A focus on screen-printed electrodes and their application," *Sensors (Switzerland)*, vol. 16, no. 10, pp. 1–16, 2016.

[22] Z. O. Ameur and M. M. Husein, "Electrochemical Behavior of Potassium Ferricyanide in Aqueous and (w/o) Microemulsion Systems in the Presence of Dispersed Nickel Nanoparticles," *Sep. Sci. Technol.*, vol. 48, no. 5, pp. 681–689, 2013.

[23] S. Cinti, V. Mazzaracchio, I. Cacciotti, D. Moscone, and F. Arduini, "Carbon black-modified electrodes screen-printed onto paper towel, waxed paper and parafilm m®," *Sensors (Switzerland)*, vol. 17, no. 10, pp. 1–12, 2017.

[24] S. Vogt, Q. Su, C. Gutiérrez-Sánchez, and G. Nöll, "Critical View on Electrochemical Impedance Spectroscopy Using the Ferri/Ferrocyanide Redox Couple at Gold Electrodes," *Anal. Chem.*, vol. 88, no. 8, pp. 4383–4390, 2016.

[25] X. Li, H. Zhao, L. Shi, X. Zhu, M. Lan, and Z. H. Fan, "Electrochemical sensing of nicotine using screen-printed carbon electrodes modified with nitrogen-doped graphene sheets," *J. Electroanal. Chem.*, 2016.

[26] E. Bianchi, F. Boschetti, G. Dubini, and C. Guiducci, "Model of an Interdigitated Microsensor to Detect and Quantify Cells Flowing in a Test Chamber.," *Cell*, no. March 2017, 2010.

[27] P. C. Pwavodi, V. H. Ozyurt, S. Asir, and M. Ozsoz, "Electrochemical sensor for determination of various phenolic compounds in wine samples using Fe3O4 nanoparticles modified carbon paste electrode," *Micromachines*, vol. 12, no. 3, 2021.